This is a repository copy of *High strain rate behaviour of cohesive soils*.

White Rose Research Online URL for this paper:
https://eprints.whiterose.ac.uk/221559/

Version: Published Version

High strain rate behaviour of cohesive soils

Arthur Van Lerberghe [*], Kin Shing O. Li, Andrew D. Barr, Sam D. Clarke

Department of Civil & Structural Engineering, University of Sheffield, Mappin Street, Sheffield, S1 3JD, UK

ARTICLE INFO

ABSTRACT

Soil-filled wire and geotextile gabions are essential components of defensive infrastructure in military bases, leveraging the attenuating properties of soils to safeguard personnel and critical assets against blast and fragmentation effects. However, understanding the behaviour of cohesive soils under extreme loading conditions remains largely unexplored, presenting a crucial knowledge gap for design engineers tasked with developing robust soil constitutive models to address evolving threats. This study investigates the response of cohesive soils, focusing primarily on kaolin clay due to its homogeneity, widespread availability and consistent properties. Through high strain rate experimental testing of kaolin clay specimens, using the split-Hopkinson pressure bar (SHPB) apparatus, both unconfined and confined conditions are explored across varying moisture contents, spanning the spectrum from unsaturated to fully saturated states. The analysis of the experimental results uncovers the strain rate dependence of cohesive soils and identifies distinct phase behaviour for transmitted and radial stresses influenced by factors such as strain rate, moisture content and confinement. Utilising LS-DYNA, and the finite element method (FEM), the SHPB tests are modelled for comparison against experimental findings. While LS-DYNA, supplemented by Smooth Particle Hydrodynamics (SPH) node modelling, provides valuable insights, significant disparities between modelled and practical results underscore the challenges inherent with the accuracy in simulating the behaviour of cohesive soils. Nonetheless, this comprehensive exploration of cohesive soil's high strain rate behaviour yields critical insights for engineers, enabling them to adapt defensive strategies to diverse threats and loading scenarios effectively.

1. Introduction

Fortification engineers face a daunting challenge: ensuring the resilience of defensive structures worldwide. Soil-filled wire and geotextile gabions, exemplified by Hesco Concertainer, stand as stalwart solutions, offering protection against the destructive forces of blast and fragmentation. The versatility and availability of soil make it an attractive defence material, facilitating the rapid and cost-effective construction of robust-barriers. However, despite its ubiquity, the high strain rate behaviour of soil remains enigmatic, especially in the context of emerging threats and evolving landscapes. As conflicts shift from sandy terrains to regions where sand may not be readily available, the need to understand and harness the potential of cohesive soils such as clay and silt becomes imperative. These cohesive materials, found across the globe, constitute the terrestrial and aquatic strata, offering promising alternative for fortifications in diverse settings.

In navigating unfamiliar terrain, fortification engineers require precise data to assess the performance of local soils and adapt their designs accordingly. The development of constitutive models capable of accommodating new soils and emerging threats necessitates comprehensive studies on soil behaviour under extreme loading conditions.

In this regard, the focus on kaolin clay, a well-researched and representative soil, provides a foundation for quantitative insights into its mechanical response. By preparing kaolin clay samples at varying moisture contents and testing them under both unconfined and confined conditions using the SHPB apparatus, this study aims to elucidate the effects of strain rate, moisture content and confinement on cohesive soils.

Blast attenuation and cohesive soils are expansive fields. The unique characteristics of cohesive soils, including their undrained behaviour, variable saturation states, and very fine particle size, pose significant challenges in evaluating their response at high strain rates. Unlike cohesionless soils, like sand, which have been extensively studied under high strain rates conditions [1–6], cohesive soils, particularly kaolin clay, remains largely unexplored in this context. This study aims to bridge this gap by delving into new frontiers of understanding, thereby paving the way for more resilient and adaptive fortification designs.

The contemporary SHPB apparatus, named after Bertram Hopkinson, originated from his method to measure the pressure generated by bullet impacts or explosive detonations [7]. Initially, the Hopkinson pressure bar consisted of a long steel bar transmitting pressure from

---

the impact, with a shorter bar serving as a momentum trap, allowing inference of pressure wave magnitude and duration.

Herbert Kolsky expanded upon this design by incorporating two bars in series, separated by a material specimen. This configuration facilitated recording of stress pulses in each bar, enabling calculation of the dynamic stress–strain response of the specimen [8]. This system, known as the split-Hopkinson pressure bar (SHPB) or Kolsky bar, remains fundamentally unchanged. By employing one-dimensional wave theory, stress pulses measured in the bars provide insights into the stress and strain histories of the two ends of the specimen [9].

Several studies utilising the SHPB apparatus have investigated the high strain rate behaviour of cohesive soils, with tests conducted up to 2500 s^{-1}, under both unconfined and confined conditions, at different moisture contents. However, these studies lacked detailed material characterisation and sample preparations of their chosen cohesive soil. This included factors such as moisture content, particle size distribution and Atterberg limits, which hindered the reproducibility of their findings and restricted comparative possibilities with other studies [10–13].

For instance, SHPB tests conducted on dry clay samples provided some insights into the effects of moisture content on cohesive soils at high strain rates [10–13]. However, artificially frozen clay samples compromised the inherent properties of moisture content in cohesive soils, rendering the results incomparable with other SHPB tests on cohesive soils [11].

Confined SHPB tests on dry clay samples were conducted, with steel jackets of different thicknesses [10], and utilising gauged steel cylindrical cages [13]. These results provided some information on the effect of confinement at high strain rates by measuring the radial stress behaviour of the sample. Yet, no comparison was made with unconfined SHPB tests on the same soil samples to determine the effect of confinement.

In contrast, high strain rate SHPB testing on cohesionless soils is more comprehensive, with clearly defined material properties prior to investigating the impact of strain rate, moisture content and lateral confinement [1–6]. This further underscores the untapped potential of novel research in comprehensively addressing the behaviour of cohesive soils at high strain rates, an area that remains largely unexplored.

Full scale trials of blast and ballistic events entail considerable costs and time investments. Consequently, numerical techniques serve as invaluable tools for modelling these events. Explosions, blast effects, and impacts are commonly simulated using dynamic software such as LS-DYNA, which incorporates the Finite Element Method (FEM) [14].

The reliability and accuracy of material models are paramount and must be verified against experimental data [15]. Typically, this involves developing a material model based on experimental properties and then comparing the results obtained from physical experiments to those of more complex simulations. Discrepancies between the experimental and modelled data indicate inaccuracies in the material model. Adjusting the inputs until the outputs align with experimental data is not a viable solution, as the model may fail to predict future material responses under different test configurations.

In FEM-based modelling, soil is often treated as a continuum with homogeneous bulk properties [16]. Since individual particles are not explicitly modelled in continuum approaches, constitutive models are employed to capture crucial bulk properties, which are typically derived from geotechnical tests.

LS-DYNA offers various modelling approaches to create constitutive numerical models for dynamic impacts on soils. These include Lagrangian with material erosion and/or mesh adaptivity, Arbitrary Lagrangian–Eulerian (ALE), and Smooth Particle Hydrodynamics (SPH) [14]. Additionally, LS-DYNA provides a range of built-in material cards for simulating soil behaviour, from basic models with compressibility curves and yield surfaces to more complex models incorporating pore water effects, strain softening & hardening, and strain effects [14].

While most finite element (FE) studies using LS-DYNA in the literature focus on buried explosives, only as small number address SHPB modelling of soils, with an even smaller subset dedicated to cohesive soils.

LS-DYNA has been employed to model high strain rate experiments on cohesive soils, including unconfined and confined SHPB tests, utilising material cards such as *MAT_SOIL_AND_FOAM, *MAT_PSEUDO_TENSOR, *MAT_FHWA_SOIL, *MAT_GEOLOGIC_CAP_MODEL as well as *MAT_MOHR_COULOMB. Experimental data is used to build ALE numerical models and comparing their results to collected test data, yielding limited accuracy [13,17,18].

These studies highlight critical issues: the lack of clear material characterisation of the investigated cohesive soil, the absence of soil shear strength data at high pressures during modelling, and evident limitations in modelling the behaviour of cohesive soils across all saturation levels.

Furthermore, SPH modelling, an innovative meshless Lagrangian numerical technique for modelling fluid equations of motion under high strain rate effects, has never been utilised in LS-DYNA for the modelling of SHPB experiments on cohesive soils. Given the dynamic nature of SHPB tests and the complex material behaviour of cohesive soils, this presents an ideal opportunity for exploration [19].

2. Material characterisation

The soil selected is defined using EN ISO 14688–1:2002 [20], as white fine CLAY (CL). For brevity, it is referred to as 'kaolin clay'. Table 1 provides an overview of the kaolin clay material properties, which are derived using the methods described in Sections 2.1–2.5.

Table 1
Overview of the kaolin clay material properties.

Soil properties	Units	Value
Primary mineral	–	Kaolinite
Particle density, ρ_s	Mg m^{-3}	2.65
Liquid Limit, LL	%	40
Plastic Limit, PL	%	25
Plastic Index, PI	%	15
D_{50}	μm	0.74
Particle sphericity	–	Low – Medium
Angularity	–	Subrounded – Subangular
Surface texture	–	Smooth

2.1. Particle mineralogy

X-ray diffraction (XRD) was carried out on the kaolin clay to establish the constituent minerals. In XRD an incident X-ray beam undergoes diffraction due to the regular atomic structure of a crystalline specimen. By measuring the intensity of diffraction at different incident angles, θ, a distinct diffraction pattern is obtained. This pattern can be compared to a database of known patterns to identify the phases present in the specimen. Phase analysis was carried out using a PANalytical Aeris diffractometer and the ICDD's Diffraction File (PDF-4+).

Fig. 1 shows the diffraction pattern of the kaolin clay. As expected, kaolinite is the primary mineral, followed by quartz. The cohesive soil used in this investigation is composed of 70% kaolinite and 30% quartz.

2.2. Particle size distribution

The particle size distribution (PSD) of the kaolin clay is assessed using the data sheet provided by the supplier, IMERYS. Fig. 2 depicts the cumulative PSD of the kaolin clay. The D_{50} of this well-graded impermeable soil is 0.74 μm, and the clay and silt contents are calculated to be 80% and 20%, respectively. The soil is therefore characterised as CLAY (CL).
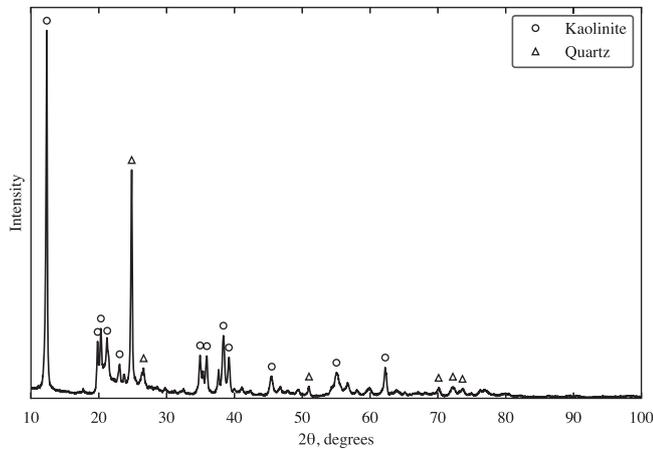
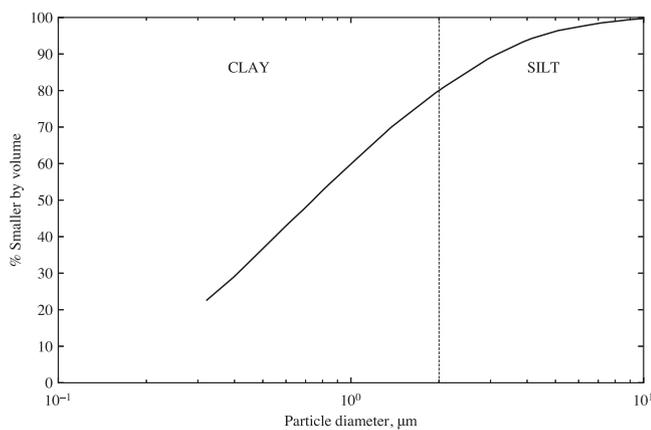**Fig. 1.** X-ray diffraction data of the kaolin clay soil.

Fig. 2. Cumulative particle size distribution of kaolin clay (from IMERYS data sheet).

Fig. 3. SEM imagery of kaolin clay at 40,000x magnification.

3. Specimen preparation

Kaolin clay samples are made using powdered speswhite kaolin clay. The powder was mixed with water at a 1:1 ratio to create a kaolin slurry, which was then placed in a pressurised cylindrical Rowe cell to consolidate the kaolin clay to 600 kPa. This approach was employed to create a consolidated, fully saturated, kaolin clay wheel, with a corresponding moisture content of 44%, as determined after preparation using the material characterisation tests indicated in Section 2.

A controlled drying procedure was utilised to study the effect of moisture content in kaolin clay samples at high strain rates. Specimens with moisture content levels of 0, 5, 10, 15, 20, 25, 30, 35, 41, 42 and 44% were prepared, covering all saturation levels from unsaturated to fully saturated. To achieve a moisture content of 0%, the samples were oven-dried for 24 h.

The kaolin clay samples used for both unconfined and confined SHPB testing are prepared using the following procedure:

1. Cylindrical kaolin clay samples with varying moisture content are made using a 25 mm stainless-steel cylinder slicer. The specimens have a nominal length of 5 mm and a diameter of 25 mm. The initial weight of the kaolin clay specimen is recorded immediately after it has been sliced.
2. Samples are air dried in a temperature-controlled setting at 20 degrees Celsius, and weighed at regular intervals to measure their current moisture content based on their initial wet weight and current weight.
3. Cut and air-dried samples are wrapped in polyvinylidene chloride to minimise changes in moisture content between sample preparation and testing. The samples are prepared and tested in different laboratories, hence they are stored in sealed plastic bags until required for testing.

4. Experimental setup

The SHPB experimental set up consists of a typical pressure bar arrangement consisting of a striker, an incident and a transmitter bar each 25 mm in diameter and 350 mm, 2500 mm and 1500 mm long, respectively, as represented in Fig. 4.The pressure bars are made of stainless steel, with the incident bar having a density of 7666 kg/m^3, a wave speed of 5376 m/s, and strain gauges with a gauge factor of 123. The transmitter bar has a density of 7677 kg/m^3, a wave speed of 5305 m/s, and strain gauges with a gauge factor of 127.

2.3. Particle density

The particle density, denoted as ρ_s, represents the density of the solid mineral particles. It is used with the bulk dry density, ρ_d, to determine the void ratio of a soil using the following relationship:

$$e = \frac{\rho_s}{\rho_d} - 1 \qquad (1)$$

The particle density, ρ_s, of the kaolin clay was calculated to be 2.65 Mg m^{-3}, using the method described in BS 1377–2:1990 §8.2 [21], which is the density of kaolinite.

2.4. Atterberg limits

To ensure sample consistency, Atterberg limits must be consistent across all soil samples. The fall cone test was used to obtain consistent Atterberg limit values for the different kaolin clay samples [21]. The liquid limit, LL, plastic limit, PL, and plastic index, PI are 40%, 25% and 15%, respectively [21]. The values of which are above the A-line, confirming the soil selected is a CLAY (CL) [22].

2.5. Particle shape

The shape of the kaolinite-sized particles in the soil are assessed qualitatively with a scanning electron microscope (SEM), using the descriptors provided in EN ISO 14688–1:2002 [20]. The kaolin clay soil was gold (Au) coated before being inserted into the SEM. Using Fig. 3, the kaolin clay particles vary from low to medium sphericity, are subrounded to subangular, and have smooth surface texture.
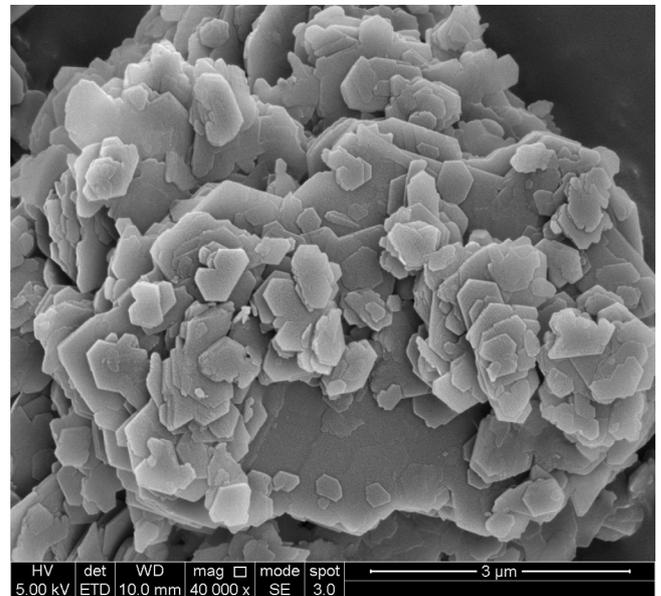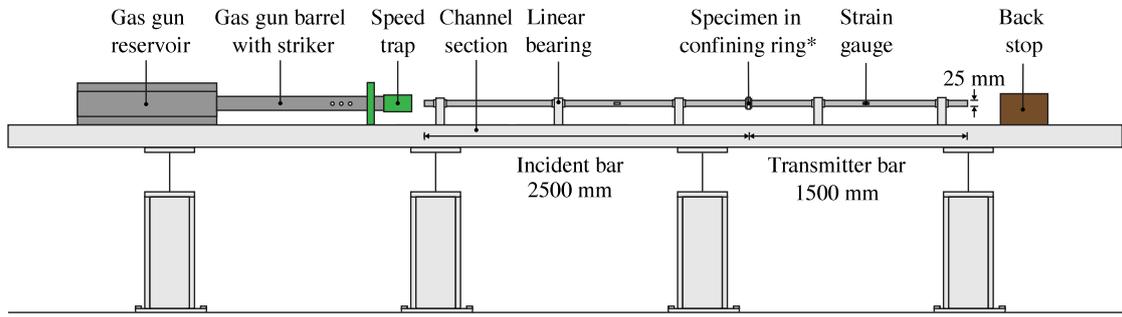
Fig. 4. Schematic diagram of the SHPB experimental setup with the confining ring [* removed for unconfined SHPB tests].

For confined SHPB testing, the experimental set up includes an additional steel confining ring shown in Fig. 5(a), which houses the kaolin clay sample and slots in between the incident and transmitter bars, as illustrated in Fig. 5(b).

Signals from the pressure bar strain gauges are recorded using a TiePie Handyscope four-channel digital oscilloscope with a 14-bit A-D resolution, a sample frequency of 1 MHz, and a record length of 131.072 kSa. The material's axial stress response is monitored using a pair of Kyowa KSP-2-120-E4 strain gauges mounted on the incident and transmitter bars. The radial stress response is measured using a single strain gauge mounted on the outside of the confining ring. Strain gauge signals are collected from the incident and transmitter bars using a half Wheatstone bridge configuration (Fig. 6). Strain gauge signal from the confining ring is acquired using a quarter Wheatstone bridge configuration (Fig. 7).

5. Testing procedure

This experimental testing procedure was used on kaolin clay samples to demonstrate the SHPB's ability to test cohesive soils under unconfined and confined conditions, as well as to validate that the chosen design set up produces reliable measurements.

Prior to testing, the samples are weighed to three decimal places using an RS Pro weighing scale, with a resolution of 0.001 g.

The samples' thickness is measured using a digital calliper at three different locations and averaged to account for any sample inconsistencies, with a resolution of 0.01 mm. These parameters are required to process the experimental data.

Unconfined SHPB testing on kaolin clay samples was conducted using the following procedure:

1. Supports surrounding the incident and transmitter bars are bolted down to the channel of the SHPB setup.
2. A kaolin clay sample 5 mm in nominal length and 25 mm in diameter was placed in between the incident and transmitter bars, inside a Perspex containment box.
3. The lid of the containment box is closed, ready for testing.

For confined SHPB testing, a similar testing procedure was followed, where the confining ring was inserted onto the incident bar before the prepared specimen is gently placed in between the incident and transmitter bars. After which, the confining ring is slid back over the specimen, ready for testing.

In both cases, loading was achieved by hitting the incident bar with a steel striker bar fired from a gas gun at varied speeds, with speeds measured using a speed trap at the exit of the gas gun barrel, to achieve different strain rates.
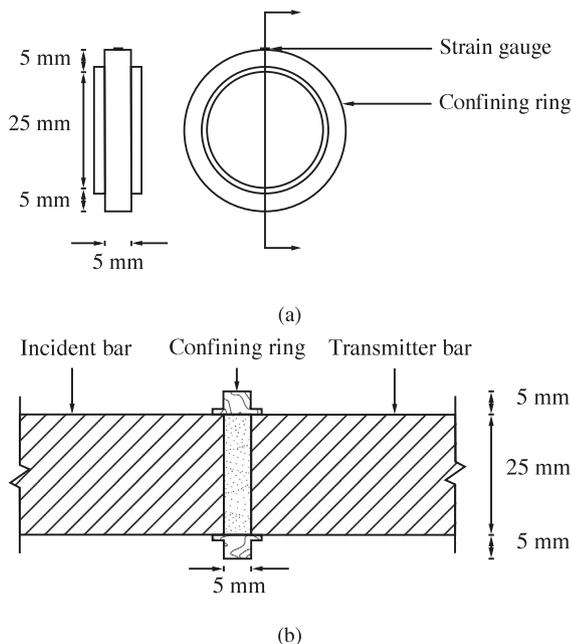

(a)

(b)

Fig. 5. Diagrams showing (a) the confining ring for confined SHPB testing and (b) the confining ring with the sample inside, ready for testing.
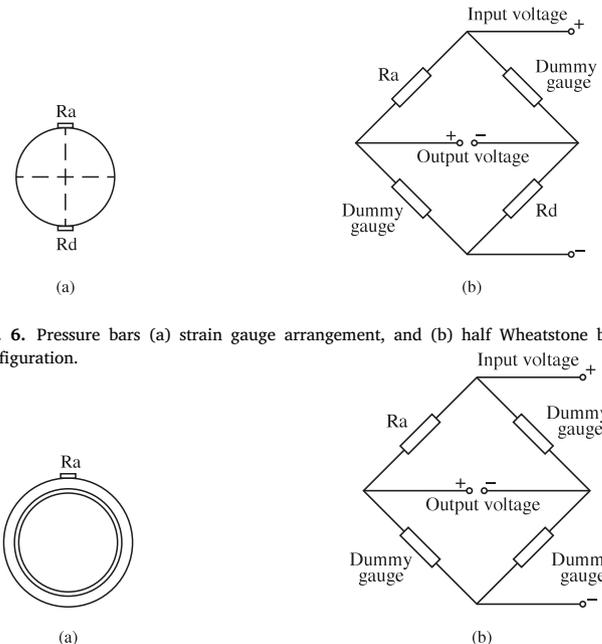

Fig. 6. Pressure bars (a) strain gauge arrangement, and (b) half Wheatstone bridge configuration.
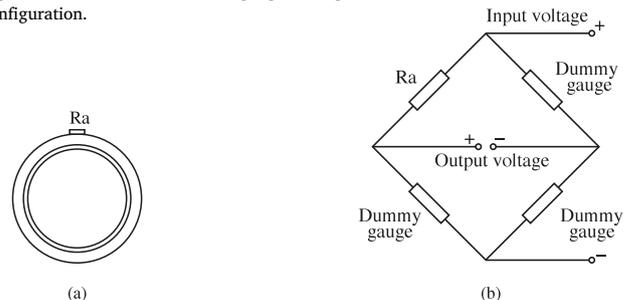

Fig. 7. Confining ring (a) strain gauge arrangement, and (b) quarter Wheatstone bridge configuration.
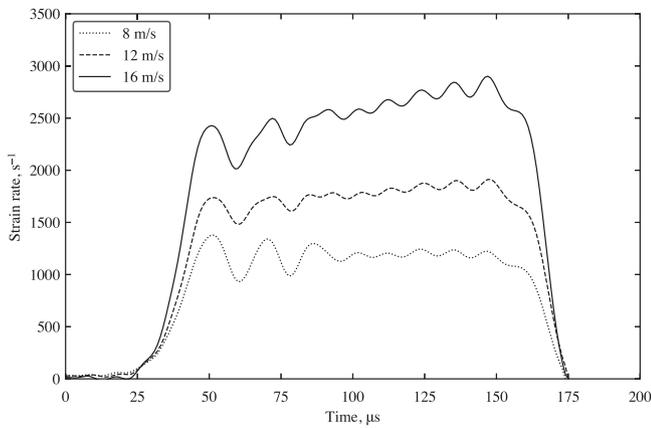
Fig. 8. Strain rate variation during unconfined SHPB testing on kaolin clay, from specific tests.
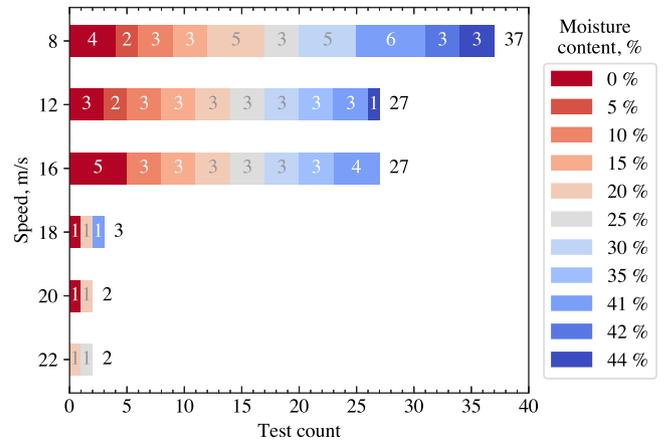

Fig. 9. Strain rate variation during confined SHPB testing on kaolin clay, from specific tests.

Fig. 10. Unconfined SHPB test programme breakdown of the number of tests for each moisture content.
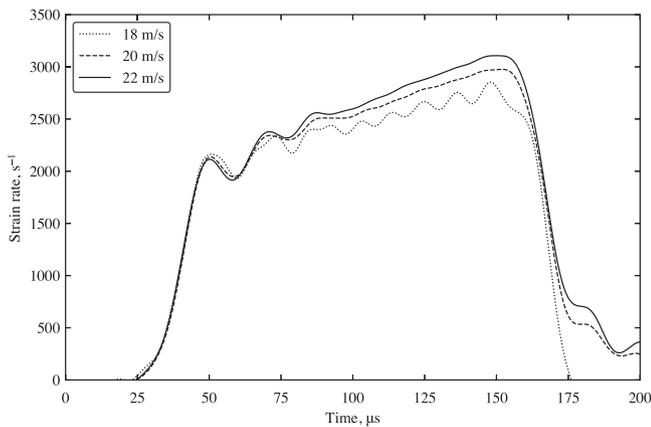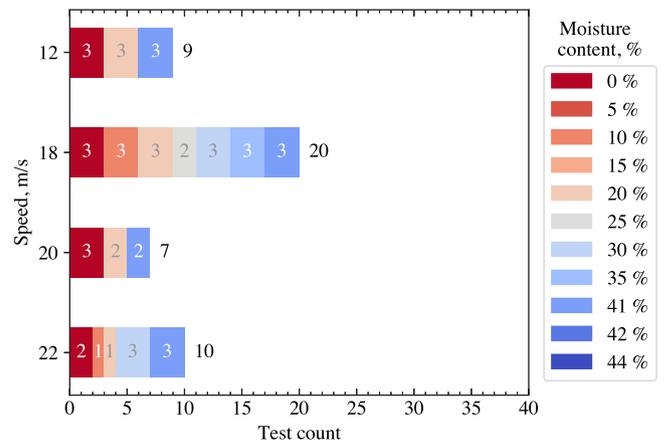

Fig. 11. Confined SHPB test programme breakdown of the number of tests for each moisture content.

6. Test programme

For unconfined SHPB testing, the test programme began with tests at 8, 12 and 16 m/s on kaolin clay samples with varying moisture content ranging from 0 to 44%. Additional tests were carried out at 18, 20 and 22 m/s to evaluate the effects of kaolin clay at higher strain rates. Under unconfined conditions, the maximum average strain rate was 1200, 1900 and 2770 s^{-1}, for 8, 12 and 16 m/s, over approximately 150 µs, as shown in Fig. 8.

For confined SHPB testing, the test programme began with tests at 12 m/s on kaolin clay samples with varying moisture content ranging from 0 to 41% for behavioural comparison with the unconfined SHPB tests. Then, tests were carried out at 18, 20 and 22 m/s. Under confined conditions, the maximum average strain rate was 2600, 2800 and 3100 s^{-1}, for 18, 20 and 22 m/s, over approximately 150 µs, as shown in Fig. 9.

At these high strain rate conditions, the specimen's axial and radial stresses and strains are measured.

The test speed utilised during SHPB testing is setup-specific and depends on the gas gun configuration selected, whereas the strain rate is what the sample experiences during testing.

Figs. 10 and 11 provide a detailed breakdown of the tested speeds, moisture contents, and corresponding number of unconfined and confined SHPB tests, respectively.

7. Signal processing

Incident bar, transmitter bar and confining ring signals gathered during SHPB tests on kaolin clay samples with varying moisture contents, are processed using the open-source Python algorithm `SHPB_Processing.py` [23], available on ORDA [24]. This code incorporates the subroutine `dispersion.py`, which implements Tyas and Pope's dispersion-correction approach. This ensures accurate representation of the sample's axial and radial stresses and engineering strains during testing [25].

To run the processing script, the amplification factors for the pressure bars and confining ring are needed. In the unconfined setup, the factors are 10 for the incident bar and 100 for the transmitter bar. In the confined setup, both bars use a factor of 10, while the confining ring is set to 5.

All plots have a fixed *y*-axis limit for clarity and ease of comparison. Although all plots start at 0, this may not be immediately visible as the *x*-axis blends with the first few data points.

To aid comparison of the waveforms, stress wave signals were truncated to match the point where the sample reached its maximum strain, after being aligned at their peak at 50 microseconds. Outside the plotted range, the stress pulses naturally start and end at 0 as expected.

Alignment based on peak stress was performed specifically for this scenario, considering the tested strains, selected material, and its non-equilibrium stress conditions. Aligning based on peak stress at smaller strains would obscure the data.

Figs. 12 and 13 show the front stress for a typical unconfined and confined SHPB test, computed using dispersion correction and simple time shifting. The 'front' stress pertains to the incident bar-clay sample interface, while the 'back' stress corresponds to the clay sample-transmitter bar interface. These figures illustrate how the dispersion-corrected approach reduces stress wave amplitude, eliminating initial fluctuations and preventing inaccurate inferences about the kaolin clay specimen's behaviour during SHPB testing. The amplitude difference between unconfined and confined SHPB tests is due to radial stresses being redirected axially by the confining ring.
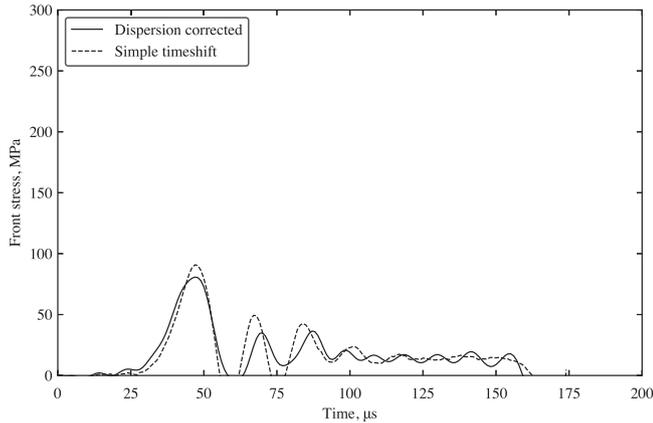

Fig. 12. Front stress computed using dispersion correction and simple timeshifting, for a typical unconfined SHPB tests on kaolin clay.
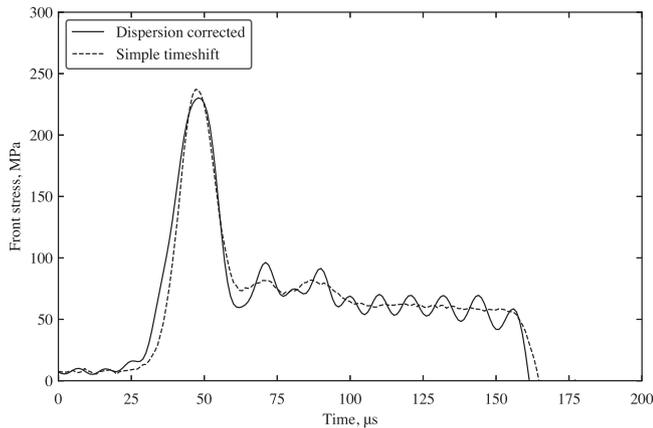

Fig. 13. Front stress computed using dispersion correction and simple timeshifting, for a typical confined SHPB test on kaolin clay.

8. Experimental results

8.1. Sample material properties

After the completion of unconfined and confined SHPB tests, the main sample properties for this study being the volume of air in the sample, V_{air}, volume of water in the sample, V_{water}, and total volume of the sample V are calculated in order to physically comprehend how the composition of air, water and soil in the sample evolved during testing.

The diameter, thickness, wet mass, and dry mass of the sample are measured prior to testing, and its moisture content is then calculated based on these values.

These properties are used to determine the volume, V, of the sample. The volume of water is determined by subtracting the dry mass from the wet mass and dividing the result by ρ_w, the density of water. The volume of solids is calculated by dividing the dry mass by the product of the specific gravity and ρ_w.

With these values, the volume of voids ($V_{voids} = V - V_{solids}$), and the volume of air ($V_{air} = V_{solids} - V_{water}$), can be calculated.

The air volume ratio in the sample is derived by dividing the total volume of air in the sample (V_{air}) by its entire volume (V), using Eq. (2):

$$\text{Air volume ratio} = \frac{V_{air}}{V} \tag{2}$$

the water volume ratio in the sample was computed by dividing the total volume of water in the sample (V_{water}) by the total volume of the sample (V), using Eq. (3):

$$\text{Water volume ratio} = \frac{V_{water}}{V} \tag{3}$$

All these geotechnical properties were determined for each sample prior to testing.

8.2. Unconfined SHPB test results

Unconfined SHPB tests were performed on kaolin clay samples with moisture content levels ranging from 0 to 44%, to cover all saturation stages: dry, partially-saturated and fully saturated. Initially, the samples were tested at 8, 12, 16 m/s, resulting in maximum average strain rates of 1200, 1900 and 2770 s^{-1}. The sample's strain, front, back and mid stresses were determined using the signal processing technique in Section 7.

Figs. 14–17 show that in a typical unconfined SHPB test at a moisture content of 0%, increasing the strain rate correlates with higher material strain, front, back and mid stresses. Fig. 16 portrays kaolin clay's strain rate dependency. A crucial discovery in our understanding of the high strain rate behaviour of cohesive soils.

At the same strain rate, the material's strain and front stress behaviour are consistent across all moisture contents. However, the back stress behaviour is dependent on the strain rate and moisture content of the tested kaolin clay sample, where it exhibits four distinct phase behaviours, as displayed in Fig. 18. This means that the material's mid stress for a specific strain rate and moisture content, is largely dependent on the measured back stress.
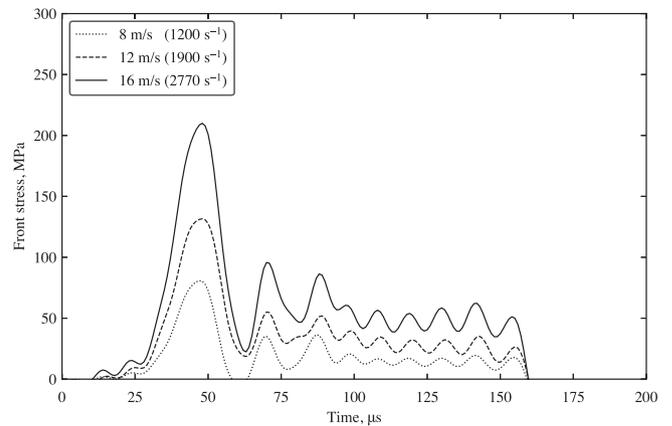

Fig. 14. Typical front stress versus time behaviour for an unconfined SHPB tests on kaolin clay, at a moisture content of 0% and different strain rates.
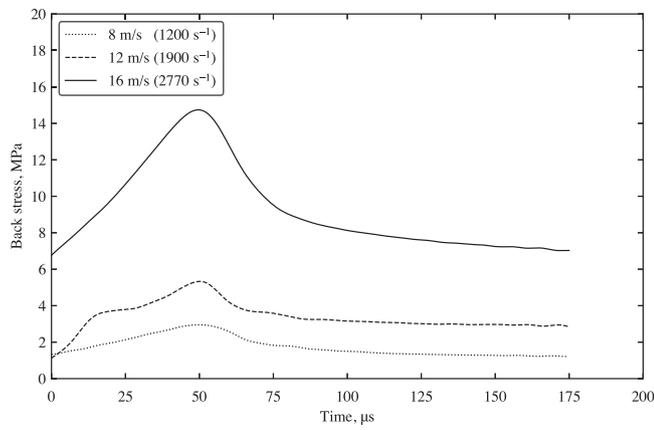
Fig. 15. Typical back stress versus time behaviour for an unconfined SHPB tests on kaolin clay, at a moisture content of 0% and different strain rates.
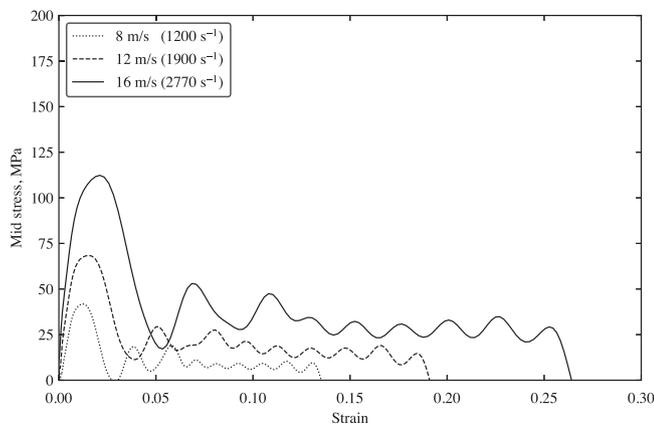

Fig. 16. Typical mid stress versus strain behaviour for an unconfined SHPB tests on kaolin clay, at a moisture content of 0% and different strain rates.
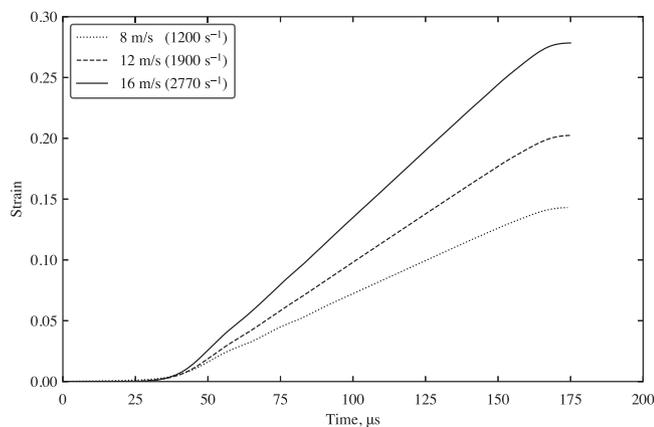

Fig. 17. Typical strain versus time behaviour for an unconfined SHPB tests on kaolin clay, at a moisture content of 0% and different strain rates.

To facilitate the analysis of experimental data collected from SHPB tests, trends in material response based on the sample's material properties were categorised, each associated with representative phase behaviours depicted in Fig. 18a, b and c. The four phases identified can be defined as follows:

- **Phase 0:** This phase includes the tests located on the *y*-axis of Fig. 18a, b and c. Samples are dry, with a moisture content of 0%. The sample no longer contains any water; it is dry, consisting mainly of air and kaolin clay. Since there is no moisture to encourage lateral extrusion of the sample in this phase, the back stress is the highest, and a larger proportion of the stress wave travels axially towards the transmitter bar. The back stress does not return to zero because the sample consolidates, leaving a thin dry kaolin disk between the bars (Fig. 18d).

- **Phase 1:** This phase is shown in red in Fig. 18a, b and c. Samples in this phase are partially-saturated throughout the test, and the soil pores are primarily filled with air. It encompasses tests with a moisture content above 0% and the intersection of the air and water volume trendlines (Point A). The back stress during this phase has a distinct shape, with a magnitude significantly lower than in phase 0, and returns close to zero after reaching its peak as the sample almost entirely extruded during testing. In phase 1, moisture content has no effect on the back stress behaviour of the kaolin clay samples (Fig. 18e).

- **Phase 2:** This phase is shown in orange in Fig. 18a, b and c. Samples in this phase are partially-saturated throughout the test but the soil pores are primarily filled with water. The range of this phase varies depending on the strain rate of the tests and correlated between the theoretical and final experimental strains. This phase spans from Point A to the intersection of the air volume ratio and the maximum experimental strain experienced by the sample during testing (Point B). In phase 2, moisture content has no effect on the back stress behaviour of the kaolin clay samples (Fig. 18f).

- **Phase 3:** This phase is shown in yellow in Fig. 18a, b and c. Samples in this phase become fully saturated during testing. This phase includes tests with a moisture content higher than the intersection of the air volume ratio and the maximum experimental strain experienced by the sample during testing (Point B). During this phase, the back stress first consists of an initial peak before levelling off and gradually decreasing back down to zero. This is due to the fast extrusion of the kaolin clay sample, which is behaving as a fluid. Within phase 3, moisture content has no effect on the back stress behaviour of the kaolin clay samples (Fig. 18g).

To create the phase diagrams in Fig. 18a, b and c, the previously calculated parameters – moisture content, water volume ratio, and air volume ratio – were plotted for each sample along with their trendlines. The maximum experimental strain for each sample, which indicates the point at which the sample becomes fully saturated and all air is removed, was recorded. Boundary lines were then added based on the intersections of these trendlines, defining the four distinct phase behaviours.

Fig. 18a, b and c show that as strain rate rises, phase 1 and 3 increase, while phase 2 decreases. This is due to the increase in the maximum experimental strain the sample experiences during unconfined SHPB testing. Additional tests performed at 18, 20 and 22 m/s have phase 2 disappearing, as the maximum experimental strain achieved a strain of 0.29, at the intersection of the two trendlines.
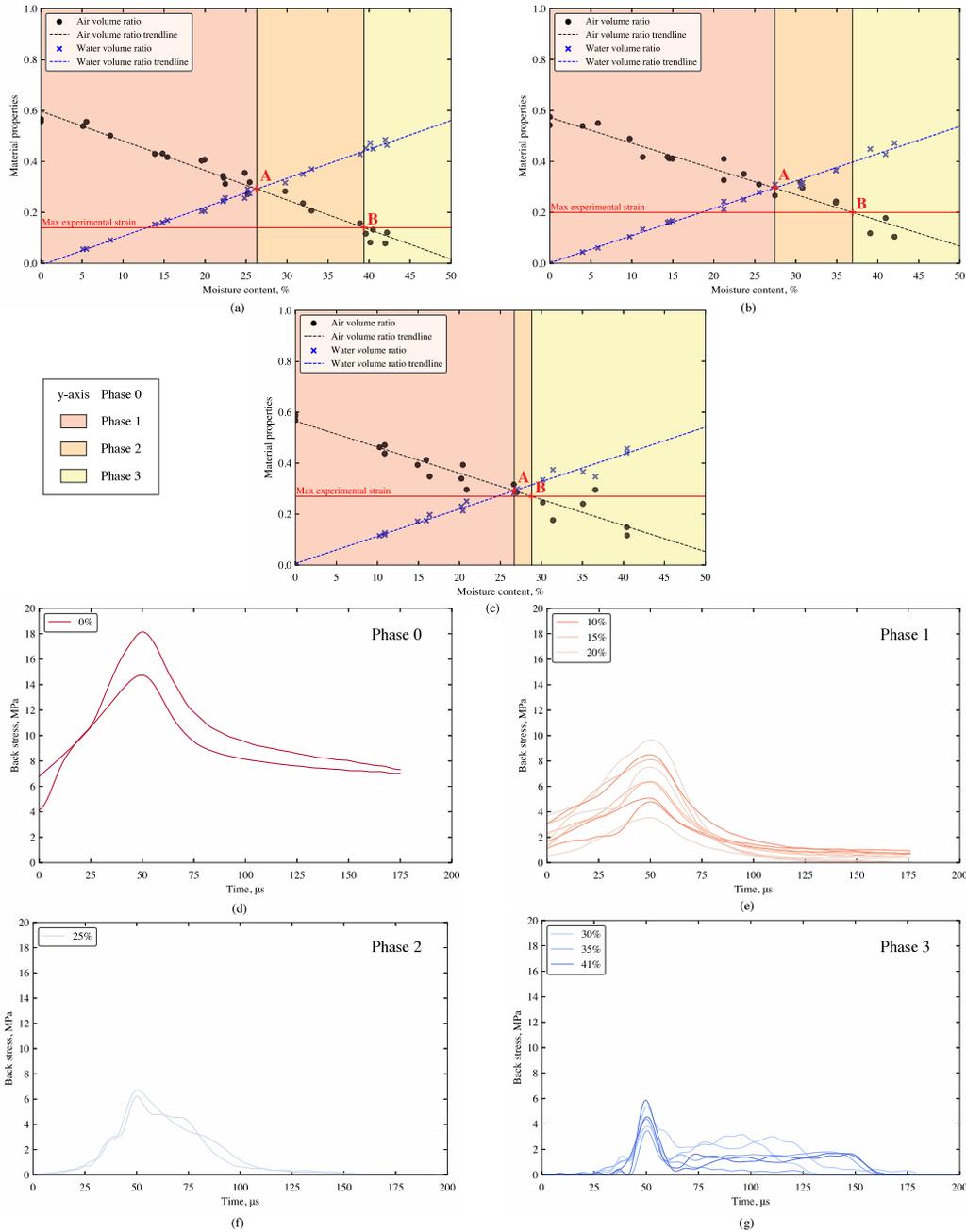
Fig. 18. Unconfined SHPB testing of kaolin clay with (a) the phase behaviour at 8 m/s (1200 s^{-1}) , (b) phase behaviour at 12 m/s (1900 s^{-1}) and (c) phase behaviour at 16 m/s (2770 s^{-1}), as well as the associated back stress at 16 m/s (2770 s^{-1}) for (d) Phase 0, (e) Phase 1, (f) Phase 2 and (g) Phase 3.

8.3. Confined SHPB test results

Applying the same processing methodology used for unconfined SHPB tests (Section 7), the sample's stress and strain data from the confined SHPB tests can be obtained. The confining ring is employed to investigate the effects of strain rate and moisture content and determine if the previously observed phase behaviour in unconfined testing persists under rigid lateral confinement.

Figs. 19–23 display the strain, radial, front, back and mid stresses for a typical confined SHPB test on kaolin clay, with 0% moisture content at different strain rates. These figures illustrate how the stress and strain responses of the sample increase with higher strain rates, while the moisture content remains constant. At a given strain rate, strain and front stress remain consistent regardless of the moisture content of the sample.

However, radial and back stresses vary depending on the sample's moisture content, directly impacting the mid stress response (Fig. 24). The mid stress versus strain response is displayed in Fig. 22. This confirms earlier findings from unconfined SHPB tests, highlighting the strain rate and moisture content dependence of cohesive soils (see Section 8.2).

Similar to the findings in unconfined SHPB tests, moisture content in the sample significantly influences the high strain rate behaviour of back and radial stresses. Fig. 24 illustrates the distinct differences in stress propagation attributed to the phase behaviour of radial and back stresses. The rigid lateral confinement provided by the confining ring acts as a barrier, restricting lateral propagation and redirecting stress axially.

The rigid lateral confinement provided by the confining ring acts as a barrier, restricting lateral propagation and redirecting stress axially.

This changes the applied loading from one-dimensional stress to one-dimensional strain. Additionally, the confining ring ensures stress wave equilibrium during testing and allows precise recording of radial stresses without deformation at high strain rates.

For fully saturated kaolin clay samples, a Poisson's ratio of 0.5 is calculated using confined SHPB test results, and gradually reduces as the sample's moisture content falls. Nevertheless, as the phase behaviour evolves from 4 to 3 phases, as seen in Fig. 24, the confining ring is unable to completely seal the sample inside. Therefore, the radial stress obtained is solely a product of the high incident stresses caused by the speed of the striker bar as it impacts the sample, causing it to extrude.
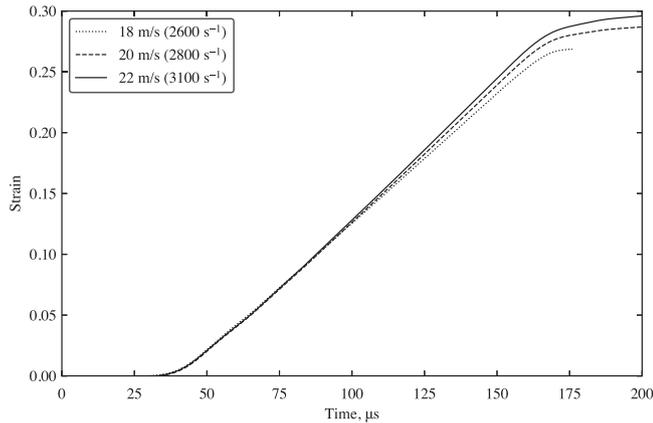
The phase diagrams in Fig. 24a, b and c for the confined SHPB tests were built using a similar manner to Fig. 18a, b and c for the unconfined SHPB tests.

Confined SHPB tests include four phases at 18 m/s (i.e 2600 s^{-1}) and three phases at 20 and 22 m/s (i.e. 2800 and 3100 s^{-1}, respectively), as seen in Fig. 24a, b and c.

In phases 0 and 1, back and radial stresses behave similarly. The back stress starts at zero, increases to a maximum, then slowly decreases before levelling off, never returning to zero (Fig. 24d and e). The radial stress reaches a similar maximum then returns to zero after 50 μs (Fig. 24g and h).

This occurs for phase 0 and 1, since the volume of water in the sample is less than its total volume of air and soil. During testing, since samples in phase 0 and 1 have a large volume of air voids, they are compacted upon impact. The sample's compaction throughout testing generates a shock absorption effect, dampening the stress wave. As a result, just a fraction of the stress wave propagates through the sample onto the transmitted bar interface. This phenomenon is caused by the confining ring. This instrument provides a rigid lateral confinement around the sample, forcing it to consolidate, resulting in a high radial stress and a totally compacted sample at the end of testing.

It is crucial to note that at the same strain rate, 2700 s^{-1}, under unconfined conditions, a SHPB test requires a striker speed of 12 m/s. Hence, speed is relative to our own test setup whereas strain rate is what the sample exhibits during testing.

Fig. 19. Typical strain versus time behaviour for a confined SHPB tests on kaolin clay, at a moisture content of 0% and different strain rates.
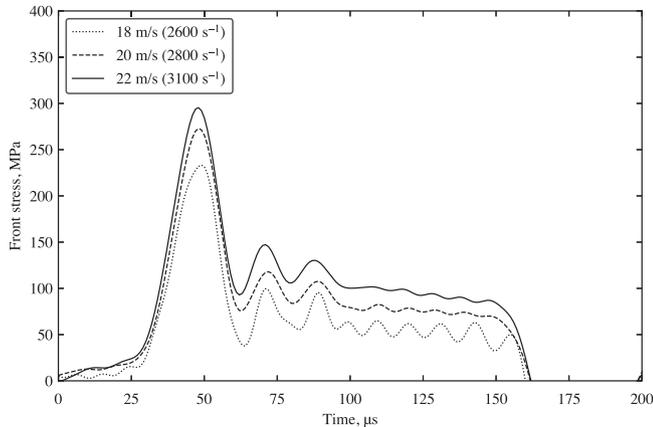

Fig. 20. Typical front stress versus time behaviour for a confined SHPB tests on kaolin clay, at a moisture content of 0% and different strain rates.
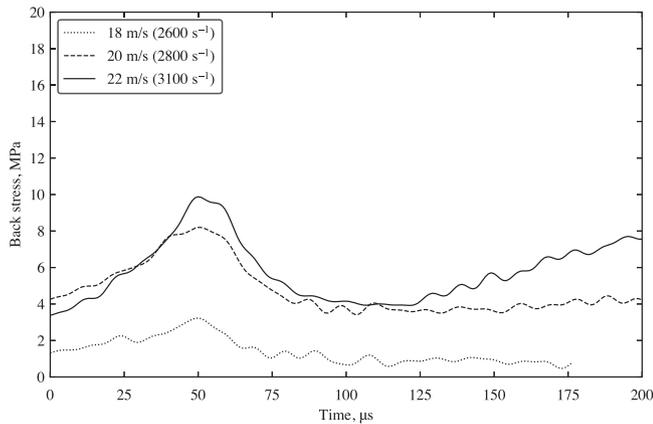

Fig. 21. Typical back stress versus time behaviour for a confined SHPB tests on kaolin clay, at a moisture content of 0% and different strain rates.
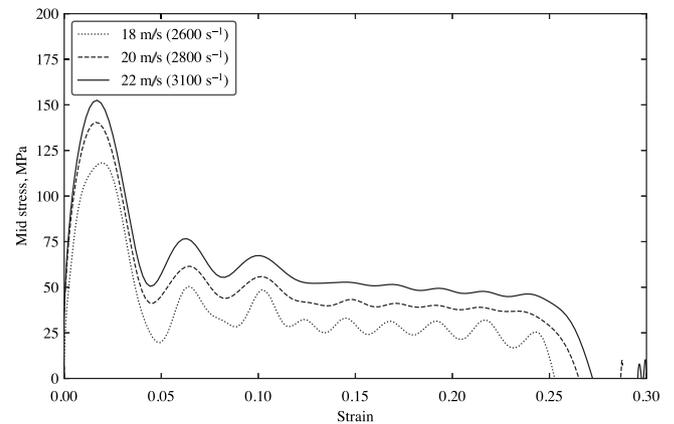

Fig. 22. Typical mid stress versus strain behaviour for a confined SHPB tests on kaolin clay, at a moisture content of 0% and different strain rates.
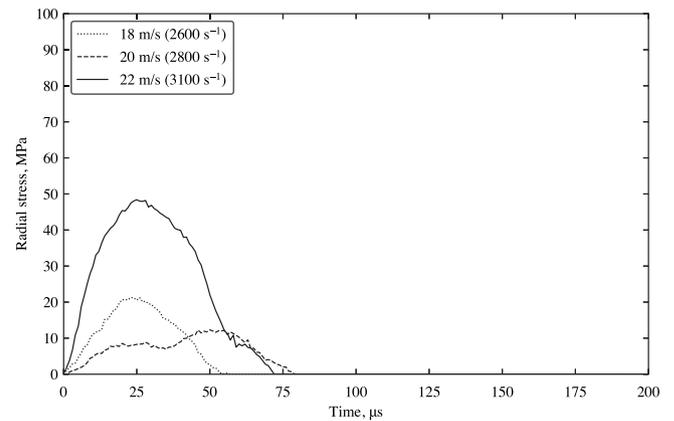

Fig. 23. Typical radial stress versus time behaviour for a confined SHPB tests on kaolin clay, at a moisture content of 0% and different strain rates.
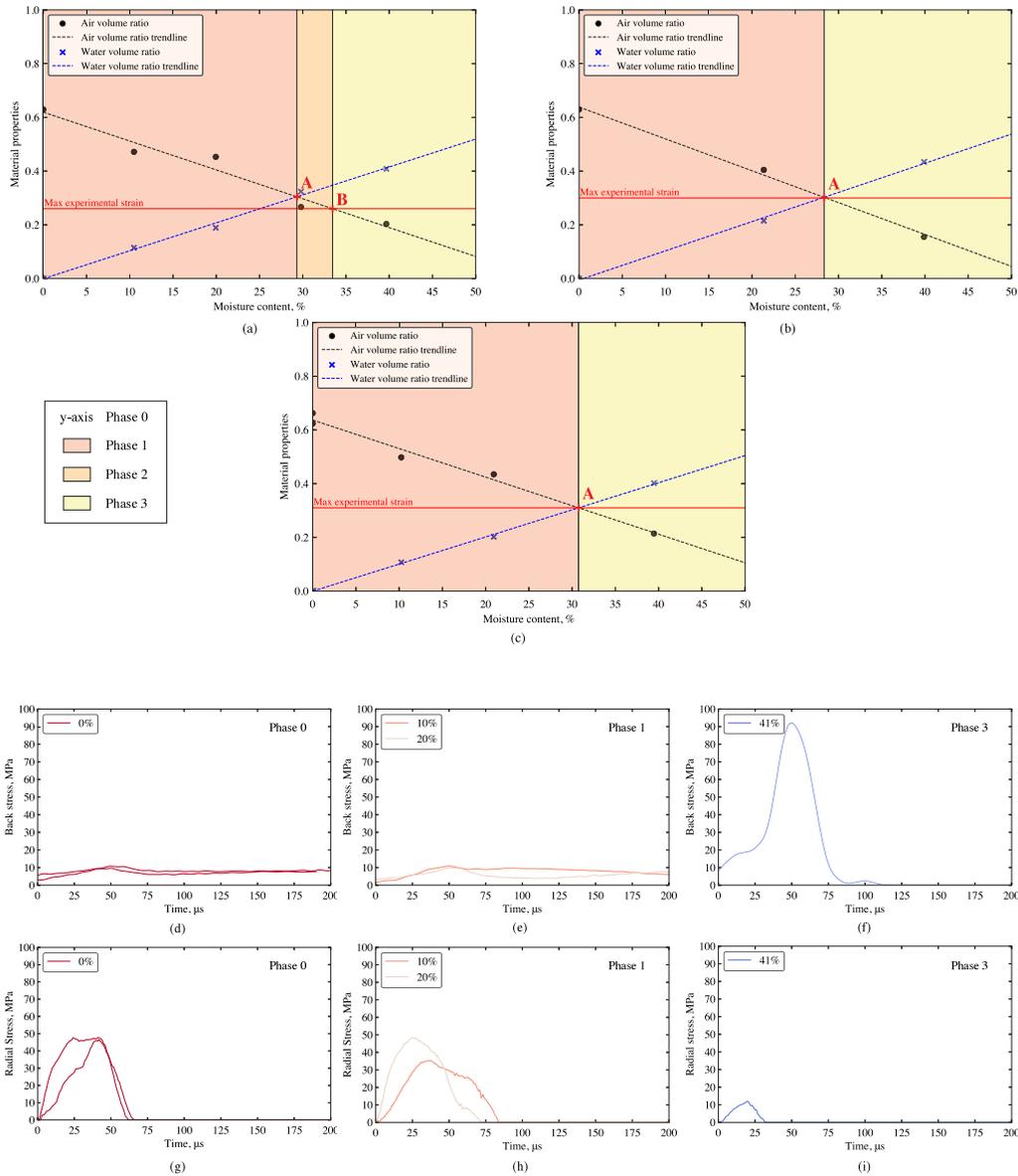
Fig. 24. Confined SHPB testing of kaolin clay with (a) phase behaviour at 18 m/s (2600 s^{-1}), (b) phase behaviour at 20 m/s (2800 s^{-1}) and (c) phase behaviour at 22 m/s (3100 s^{-1}), as well as the associated back stress at 20 m/s (2800 s^{-1}) for (d) Phase 0, (e) Phase 1, and (f) Phase 3, and radial stress at 20 m/s (2800 s^{-1}) for (g) phase 0, (h) phase 1, and (i) phase 3.

Phase 2 manifests only in the confined SHPB tests at 18 m/s (equivalent to 2600 s^{-1}). However, it completely vanishes when the sample's maximum experimental strain reaches 0.29, occurring at a strain rate of 2700 s^{-1} (Point B equals Point A), a finding empirically validated. Consequently, Phase 2 is conspicuously absent at higher velocities of 20 and 22 m/s (i.e. 2800 and 3100 s^{-1}, respectively), as shown in Fig. 24a, b and c.

Fig. 24f and i illustrate the discernible back and radial stress behaviours characteristic of phase 3 compared to other phases. Beyond a strain rate of 2700 s^{-1}, following the disappearance of phase 2, the impact of the incident bar, the effect of inertia, becomes significant enough to prompt the sample extrusion, irrespective of confinement.

Similar to unconfined experiments, once the moisture content surpasses the threshold for the specimen to achieve full saturation, the water content ratio dictates the sample's behaviour, leading to complete lateral extrusion.

In theory, the confining ring forms a tight seal around the pressure bars, ostensibly preventing sample extrusion. However, in practice, kaolin clay particles still undergo extrusion beyond a certain strain rate due to the substantial impact caused. The confining ring's influence on stress wave propagation in cohesive soils is underscored by several intrinsic factors.

Table 2
Material card for *MAT_MOHR_COULOMB, calibrated for use with kaolin clay [14].

*MAT_MOHR_COULOMB							
$#	mid	ro	gmod	rnu	phi	cval	psi
	X	x1	1.3E7	x2	0.08075	55759.4	0.0
$#		nplanes		lccpdr	lccpt	lccjdr	lccjt	lcsfac
		0		0	0	0	0	0
$#	gmoddp	gmodgr	lcgmep	lcphiep		lcgmst	cvalgr	aniso
	0.0	0.0	0.0	0.0		0.0	0.0	1.0

x1 and x2 are adjusted based on the material properties of the sample tested.

9. Numerical modelling of SHPB tests

9.1. Model setup

The numerical model of the setup is shown in Fig. 25. It was created using the FEM software LS-DYNA, in order to compare numerical and experimental SHPB test results on kaolin clay samples. The striker (yellow in Fig. 25), incident (blue in Fig. 25) and transmitter (green in Fig. 25) bars are modelled as 3D solid Lagrangian meshes. The confining ring (orange and pink in Fig. 26(b)) is also modelled this way. SPH node modelisation was used for the kaolin clay sample.

Fig. 26(a) depicts the 5 mm SPH kaolin clay sample section numerically simulated between the incident and transmitter bars. A more detailed representation of the confining ring with the SPH sample slotted inside is illustrated in Fig. 26(b). A fixed sample length of 5 mm was chosen, and the model's bulk density was changed to match the precise sample length tested using the SHPB apparatus.

When examined at high strain rates, kaolin clay exhibits high deformation and fluid-like behaviour, hence SPH is chosen as the most suitable option over traditional ALE or Lagrangian meshing procedures. Consequently, there are no problems associated with excessive distortion or negative volume errors.

The contact interface between the SPH-modelled kaolin clay sample and the two Lagrangian pressure bars (i.e. incident and transmitter bar) was represented in LS-DYNA using the automated nodes-to-surface contact interaction. The contact interface between the SPH-modelled kaolin clay sample and the inside of the confining ring was modelled in this similar manner, using automated nodes-to-surface contact interaction.

The interfaces between the striker-incident bar, and incident-transmitter bar are modelled using manual surface-to-surface contact interactions.

9.2. Model material cards

The stainless-steel pressure bars are modelled as linear elastic using the *MAT_ELASTIC, with a density, Young's modulus and Poisson's ratio of $\rho = 7666$ kg m^{-3}, E = 222 GPa and $\nu = 0.29$, respectively. To mirror the experimental tests, the model's striker bar velocity was set to the associated striker speed used in experimental testing: 8, 12, 16 m/s for unconfined SHPB tests and 18, 20, 22 m/s for confined SHPB tests.

The confining ring used for SHPB testing is made of stainless-steel. It was initially modelled as linear elastic using *MAT_ELASTIC, however, this led to a lot vibration and noise interference with the numerical data. A fully rigid confining ring was modelled using the *MAT_RIGID to remove these interferences associated with the contact between the pressure bars and the confining ring. This resulted in no radial stress data being recorded. Therefore, a combination of rigid and elastic elements were utilised to model the confining ring to be able to collect radial stress data (orange and pink in Fig. 26(b)).

The kaolin clay sample made using SPH was modelled with *MAT_MOHR_COULOMB, which has a bulk density (ro), elastic shear modulus (gmod), Poisson's ratio (rnu), angle of friction (phi) and cohesion factor (cval). The bulk density (ro) and Poisson's ratio (rnu) vary depending on the moisture content of the kaolin clay sample examined.

Unconfined undrained triaxial (UU TXC) tests were conducted on fully saturated kaolin clay to populate the LS-DYNA model using known quasi-static parameters. The angle of friction, phi, was estimated by plotting Mohr's circles and adjusting the stress envelope slightly above horizontal to avoid a zero value for phi, which would cause model failure. This provided phi = 4.62° (0.08075 rad). The cohesion factor, cval, was determined from the same plots, yielding a value of 55,759.4 Pa. The elastic shear modulus, gmod, was calculated as 1.3E7 Pa. The initial density (ro) and Poisson's ratio (rnu) were adjusted for each sample and are listed as x1 and x2 in Table 2. All these parameters are summarised in Table 2.

Fig. 25. LS-DYNA SHPB model set up with the confining ring [The confining ring is removed for unconfined SHPB modelisation].
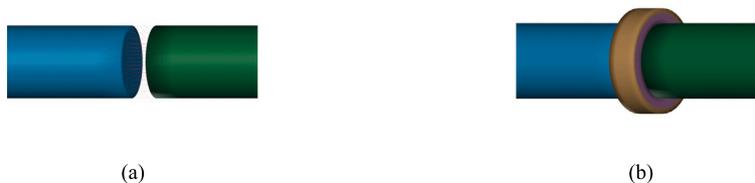

(a)

(b)

Fig. 26. LS-DYNA zoom-in on modelling for (a) the unconfined SHPB setup, and (b) the confined SHPB setup.

9.3. Comparison between unconfined SHPB tests and corresponding LS-DYNA numerical models

The material card `*MAT_MOHR_COULOMB` incorporates the bulk density, ρ, and Poisson's ratio, ν, based on the moisture content of the sample being modelled. These parameters are designated as `x1` and `x2` in Table 2.

Table 3 provides a comprehensive overview of the inputs utilised in LS-DYNA to model the unconfined SHPB tests, along with the corresponding results, specifically the maximum front and back stresses within the model. Twelve distinct unconfined SHPB model setups were executed, each with varying input parameters, such as striker speed, moisture content, bulk density (ρ) and Poisson's ratio (ν).

Test number 6 highlighted a critical issue: inputting a Poisson's ratio of 0.5 in the `*MAT_MOHR_COULOMB` material card resulted in failure. The Poisson's ratio is a crucial parameter necessary to accurately simulate the fluid-like behaviour of kaolin clay under high moisture content and high strain rates (Table 3).

Test results also indicated that inputting a Poisson's ratio of 0.40, 0.44 or 0.49 yielded identical maximum front and back stresses as noticed across tests no. 1, 2 and 3. Similarly, the variation in bulk density within the sample, intended to simulate different moisture content levels, had no effect on the output, as demonstrated by the consistent maximum front and back stresses observed in tests 2, 4 and 5 (Table 3).

The incident and reflected pulses as well as the back stress obtained from the LS-DYNA numerical models are compared against the experimental SHPB test data collected, as illustrated in Figs. 27–29.

Figs. 27 and 28 juxtapose the typical experimental and numerical incident and reflected pulses obtained for a striker speed of 8 m/s (1200 s^{-1}). The shape of the incident pulse in the numerical model still mirrors a similar pattern to the experimental results. However, there is a notable difference in the reflected pulse behaviour. While experimentally, the incident pulse propagates through the sample, in the LS-DYNA numerical model, the incident pulse is completely reflected, indicating that the stress wave is unable to propagate through the SPH sample in the model. As a result, the computed front stress is significantly lower than the experimental results.

Fig. 29 illustrates a notable disparity between the back stress in LS-DYNA and the experimental back stress. This disparity arises because the incident pulse is entirely reflected upon contact with the sample. Upon impact from the incident bar, the SPH particles in LS-DYNA eject both axially and laterally as the stress wave propagates through the kaolin clay sample. Consequently, the particle cohesion properties of the specimen do not contribute to the stress wave's propagation into the transmitted bar.

Despite the limitations in LS-DYNA in modelling cohesive soils at high strain rates, tests number 2, 4, 5, 7, 8, 9, 10, 11 and 12, conducted at speeds of 8, 12 and 16 m/s, demonstrated that as the strain rate increases so does the maximum front and back stresses. This indicates that these LS-DYNA models still adequately capture the effect of strain rate in cohesive soils at high strain rate.

9.4. Comparison between confined SHPB tests and corresponding LS-DYNA numerical models

The same material card is used to model the confined SHPB tests in LS-DYNA, `*MAT_MOHR_COULOMB`. Similarly to the unconfined SHPB models, Table 3 provides an overview of the inputs utilised in LS-DYNA to model the confined SHPB tests, along with the corresponding outputs, specifically the maximum front, back and radial stresses from the model.

Tests 13 to 24, detailed in Table 3, echo the findings of unconfined SHPB models, confirming that Poisson's ratio does not influence the results, with the model failing to run for a Poisson's ratio of 0.5. Furthermore, adjustments in moisture content through variations in bulk
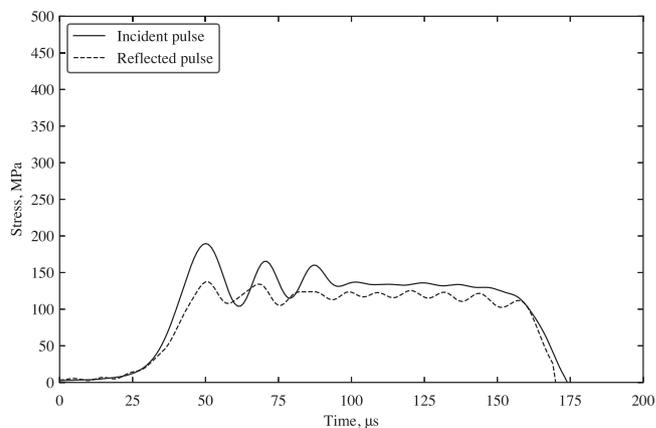

Fig. 27. Typical stress behaviour from the incident and reflected pulses of an unconfined SHPB experimental test, at 8 m/s (1200 s^{-1}).

Fig. 28. Typical stress behaviour from the incident and reflected pulses of an unconfined SHPB tests in LS-DYNA, at 8 m/s (1200 s^{-1}).

Fig. 29. Comparison of back stress from the experimental unconfined SHPB tests and corresponding numerical LS-DYNA models on kaolin clay at a moisture content of 0% and different strain rates.

density, observed in model tests 13 to 24, do not alter the material's behaviour in the model.

Figs. 30 and 31 depict the incident and reflected pulses in the experimental tests and numerical model. The front stress behaviour in the LS-DYNA numerical model resembles that observed in the SHPB tests, albeit with a higher magnitude due to the sample containment seal in the numerical model setup of the confining ring (Table 3).

Table 3
Summary of the LS-DYNA modelling inputs and outputs.

Test No.	Striker speed m/s	Moisture content %	ρ (ro) kg m^{-3}	ν (rnu)	Max front stress MPa	Max back stress MPa	Max radial stress MPa
Unconfined SHPB modelling							
1	8	0	934	0.40	21.4	2.3	–
2	8	0	934	0.44	21.4	2.3	–
3	8	0	934	0.49	21.4	2.3	–
4	8	20	1087	0.44	21.4	2.3	–
5	8	41	1296	0.44	21.4	2.3	–
6	8	41	1296	0.50	FAIL	FAIL	–
7	12	0	934	0.44	32.8	3.4	–
8	12	20	1087	0.44	32.8	3.4	–
9	12	41	1296	0.44	32.8	3.4	–
10	16	0	934	0.44	44.8	4.0	–
11	16	20	1087	0.44	44.8	4.0	–
12	16	41	1296	0.44	44.8	4.0	–
Confined SHPB modelling							
13	18	0	934	0.40	324.4	394.3	509.0
14	18	0	934	0.44	324.4	394.3	509.0
15	18	0	934	0.49	324.4	394.3	509.0
16	18	20	1087	0.44	324.4	394.3	509.0
17	18	41	1296	0.44	324.4	394.3	509.0
18	18	41	1296	0.50	FAIL	FAIL	FAIL
19	20	0	934	0.44	365.1	432.6	624.0
20	20	20	1087	0.44	365.1	432.6	624.0
21	20	41	1296	0.44	365.1	432.6	624.0
22	22	0	934	0.44	410.3	481.3	674.0
23	22	20	1087	0.44	410.3	481.3	674.0
24	22	41	1296	0.44	410.3	481.3	674.0

'–': Data not recorded, 'FAIL': LS-DYNA model failed to run.
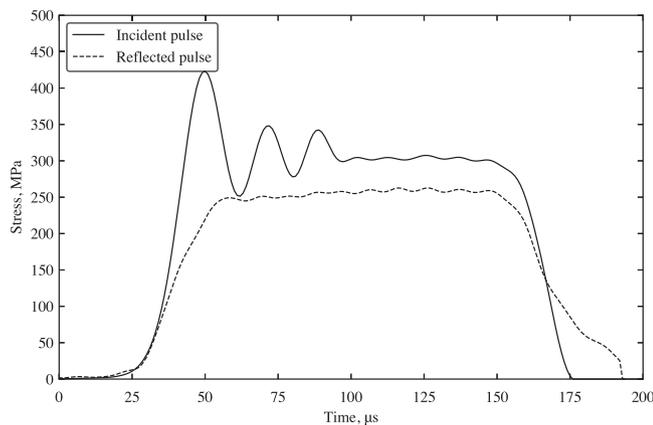
Fig. 30. Typical stress behaviour from the incident and reflected pulses of a confined SHPB experimental test, at 18 m/s (2600 s^{-1}).

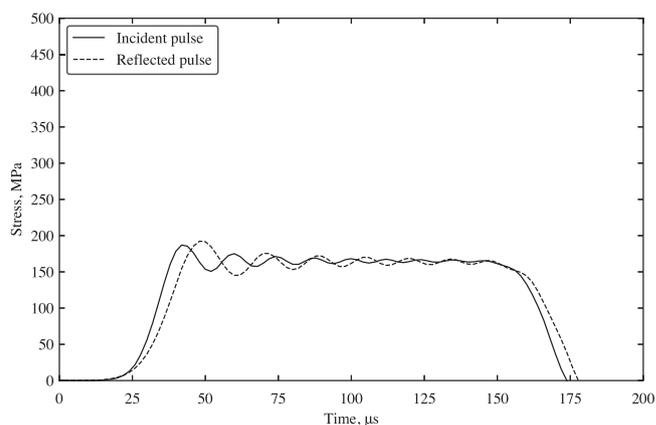**Fig. 31.** Typical stress behaviour from the incident and reflected pulses of a confined SHPB tests in LS-DYNA, at 18 m/s (2600 s^{-1}).

Back and radial stresses are shown in Figs. 32 and 33. The magnitudes of these stresses are considerably higher than those obtained from experimental testing. This is primarily due the confining ring's influence in LS-DYNA and its modelling approach, since the confining ring effectively seals the SPH specimen inside, preventing extrusion during testing. Nevertheless, the model does not accurately reflect the genuine behaviour of cohesive soils, as neither moisture content nor Poisson's ratio affects the model outputs.

The back stress results from the numerical models show an increasing trend, consistent with observations from SHPB testing. Additionally, the radial stress results from the models exhibit also an increasing trend as speed increases (Table 3).

When the sample is fully saturated, with a Poisson's ratio of 0.5, the model fails to run due to limitations of *MAT_MOHR_COULOMB, necessitating the used of *MAT_NULL to model the fluid-like behaviour of the material. Since there is no sample extrusion in the numerical model, the front, back and radial stress results show higher values than in the experimental SHPB tests (Table 3). The perfect seal of the ring in the model alters the sample's radial stress behaviour, as there is no inertia effect from the incident bar impacting the sample. Hence, the radial stress does not fall due to excessive sample extrusion from the ring, before rising again, as seen in testing.
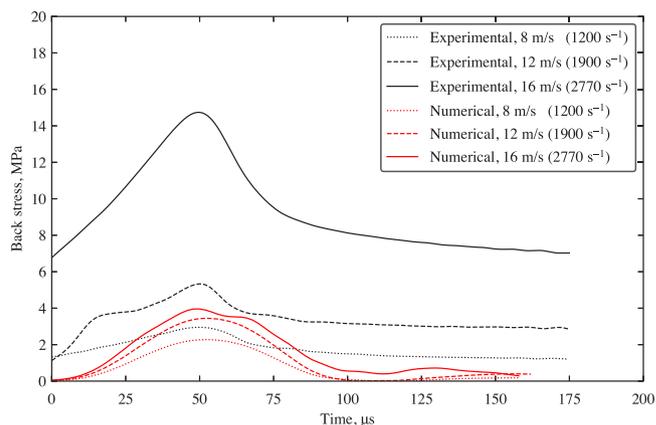
Fig. 32. Comparison of back stress from the experimental confined SHPB tests and corresponding numerical LS-DYNA models on kaolin clay at a moisture content of 0% and different strain rates.

Fig. 33. Comparison of radial stress from the experimental confined SHPB tests and corresponding numerical LS-DYNA models on kaolin clay at a moisture content of 0% and different strain rates.
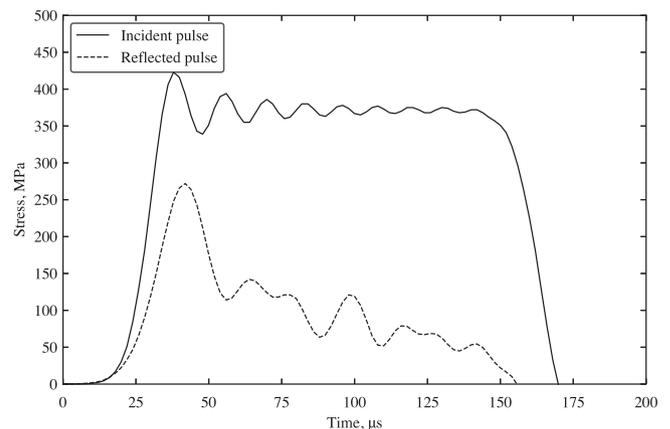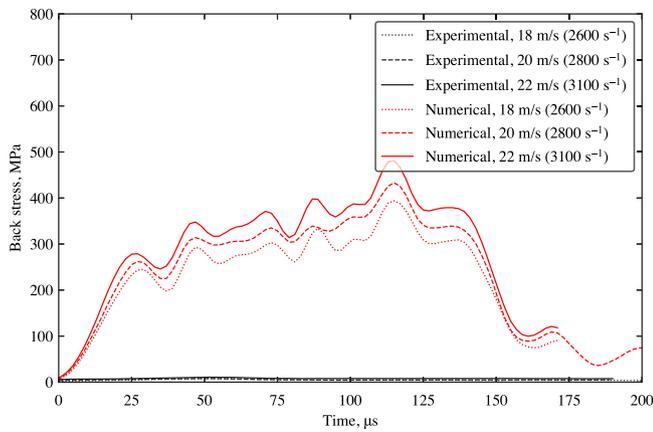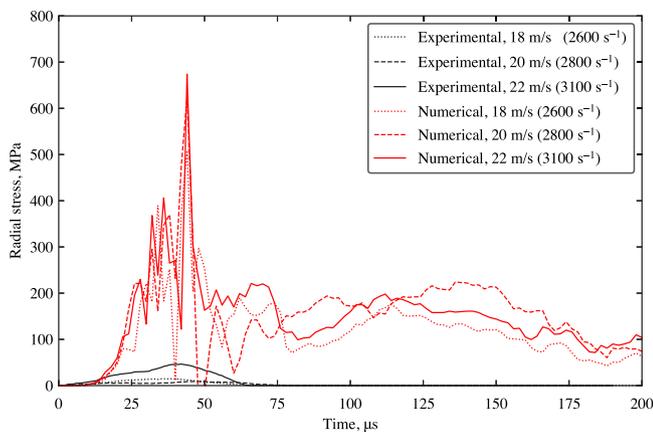
9.5. LS-DYNA modelling limitations

Notable LS-DYNA modelling limitations are as follows:

1. The difficulty in computing a compression curve due to the material's inability to endure multi-axial compression without extrusion. Since kaolin clay is strain rate dependent, there are no equations of state currently implemented into numerical simulation codes that take account of the complete time- or frequency-dependence of the mechanical response of cohesive soils. Most soil specific and cohesion material models in LS-DYNA require an EOS, therefore the list of material models which could be utilised with the parameters we collected is very short, leaving *MAT_MOHR_COULOMB as the most suitable option.

2. During the comparison of experimental SHPB test data and associated LS-DYNA numerical models, the impact of the material's moisture content could not be observed in the numerical model. Therefore, the phase behaviour could not be mapped out in LS-DYNA. This is due to the model's limitations in modelling cohesive soils at high strain rates.

3. The development of the SPH node modelisation technique in LS-DYNA is limited. LS-DYNA is unable to accurately represent the cohesion properties of cohesive soil particles. The deficiency, compounded by the lack of cohesion properties in this node modelisation tool, hinders the ability to accurately model the high strain rate behaviour of cohesive soils [26].

4. The numerical modelling of the confining ring revealed constraints related to sample extrusion, seal, vibration and contact, hence it required adjustments. Experimentally, an elastic stainless-steel ring was used to obtain the radial stress behaviour of the tested specimen, but its excessive deformation compromised accuracy. Therefore, a rigid-elastic confining ring was created to fully confine the sample, maintain stress equilibrium, prevent sample extrusion with a tight seal, and record radial stresses without complete deformation. The rigid element is 1/3 the thickness of the ring on the outside, while the elastic element is 2/3 the thickness on the inside, in contact with the SPH sample. Nevertheless, the perfect seal of the confining ring affects the stress results produced from the model, making them greater than they should be.

10. Discussion

The effect of moisture content on the behaviour of cohesive soils was thoroughly investigated through SHPB tests conducted under both confined and unconfined conditions, revealing an inherent phase behaviour. This phase behaviour significantly impacts the use of cohesive soils, as moisture content directly affects the material's ability to propagate stress. Moisture content levels in phase 1 yielded the most effective results in preventing stress wave propagation in confined test cases, while in unconfined test cases, phase 4 was the most effective.

In unconfined SHPB testing, phase 4 sees the behaviour of the material governed by the water volume in the specimen. In unconfined testing scenarios, stress propagation through the material is primarily limited by moisture content, while any remaining stress propagates laterally as the specimen extrudes. However, implementing this in practice poses challenges due to the difficulty in transporting and moulding the material into specific structures.

In confined SHPB testing, phase 1 sees the material's physical behaviour dictated by the soil, as the volume of soil in the sample exceeds that of water. In contrast to other phases, where the water volume ratio is either nonexistent (phase 0) or dominant (phases 2 and 3), phase 1 sees the water volume in the sample aiding to the material's strengthening. In cases where a confining ring restricts lateral propagation, stress is redirected axially, resulting in an increase in axial stress, as seen in phase 4 for confined SHPB tests. When phase 2 disappears, radial stress initially drops but then rises again due to inertia effects from the incident bar, resulting in sample extrusion. This indicates that the confining ring is unable to contain the sample at such high strain rate levels. Moreover, differing speed and strain rate between unconfined and confined SHPB tests underscored confinement's impact kaolin clay's high strain rate behaviour. The stress–strain analysis of the sample revealed a clear strain rate dependence of the material at high strain rates.

Given the high strain rate conditions of this research, SPH node modelisation was chosen to model the kaolin clay sample, due to its suitability for high-impact high-deformation scenarios. However, the material's strain rate dependency posed challenges in modelling the SHPB tests using LS-DYNA, as no suitable material cards were available. The absence of dedicated material cards for cohesive soil modelling in LS-DYNA complicated the depiction of observed behaviour during testing. Consequently, a general material card *MAT_MOHR_COULOMB, was used to model the kaolin clay.

In the unconfined SHPB models, the incident pulse closely matched that of the SHPB tests, validating the model setup. However, the reflected pulse exhibited considerable differences, resulting in lower front and back stress responses, attributable to the stress wave's inability to propagate through the sample. The SPH particles dissipated instantly upon contact with the incident pulse. In the confined SHPB models, the front, back and radial stresses are considerably higher than those obtained from the SHPB tests, since the confining ring provides a

perfect seal in the model enabling the stress wave to propagate through the sample more easily, resulting in considerably greater values. The rising trend observed for the front and back stresses in testing was also noticed in the model. The radial stresses obtained in the model, using a composite half-rigid, half-elastic confining ring with a perfect seal, significantly surpass those observed in testing. This is because the numerical model is a perfect test representation from which to obtain the radial stress, therefore it is unable to capture the inertial effect from the incident bar.

Comparing the tests to the numerical models for kaolin clay samples with varying moisture contents, it was observed that the variation in moisture content in model failed to demonstrate the same phase behaviour. The discrepancy can be attributed to LS-DYNA's limitations in modelling cohesive soil properties accurately, leading to erroneous modelling findings.

Given the proven limitations of LS-DYNA demonstrated in this paper, other FEA packages, such as ABAQUS using material models such as Cam-Clay [27], may be worth exploring for modelling the high-strain-rate behaviour of cohesive soils.

In conclusion, cohesive soils' ability to limit stress propagation is clearly influenced by moisture content and confinement. The SHPB test derived back stress indicates the stress that can propagate through the sample, with moisture content acting as a dampener that impedes lateral stress propagation. Confinement restricts lateral extrusion, redirecting radial stress axially and consequently affecting stress transmission through the sample.

11. Summary

In this study, the high strain rate behaviour of cohesive soils was investigated using the SHPB apparatus. A comprehensive material characterisation analysis was conducted on the chosen cohesive soil, kaolin clay. High strain rate SHPB tests were performed on kaolin clay samples with different moisture content levels under both unconfined and confined conditions. The experimental results emphasise the novelty of this research, revealing that strain rate, moisture content and confinement all influence the behaviour of cohesive soils at high strain rates. The presence of a soil phase behaviour based on the sample's moisture content was identified, as evidenced by the back stress for the unconfined SHPB tests and the radial and back stresses for the confined SHPB tests.

The FEM software LS-DYNA was used to simulate the unconfined and confined SHPB tests performed on kaolin clay samples at varying moisture contents. While modelling the test setup posed no significant challenges, clear limitations were observed in LS-DYNA when comparing experimental and numerical results: there is no dedicated material card model for cohesive soils, no cohesive properties in the software and very limited use of SPH for modelling the high strain rate behaviour of cohesive soils. These findings underscore the existing gap in modelling the high strain rate behaviour of cohesive soils.

Future endeavours in this field will initially focus on developing data-driven parametric models using all the experimental test data collected. This will enable the prediction of the unconfined and confined behaviour of cohesive soils, at high strain rates within the explored range, thereby saving considerable time and costs. Subsequently, in light of the discussed modelling limitations, there is a clear need for improvements in modelling the high strain rate behaviour of cohesive soils. To address this, experimental test data will be utilised to develop a hybrid twin model that incorporates all SHPB test results, enriching the numerical model.

Furthermore, the effect of confinement was explored by comparing a free-field unconfined scenario with a rigid confined SHPB test scenario. However, an intermediate case remains unexplored, which would assess the impact of confining pressure on lateral and axial stress propagation. This avenue presents an opportunity for further investigation.

CRediT authorship contribution statement

Arthur Van Lerberghe: Writing – review & editing, Writing – original draft, Methodology, Investigation, Formal analysis, Conceptualization. **Kin Shing O. Li:** Investigation, Formal analysis, Conceptualization. **Andrew D. Barr:** Writing – review & editing, Supervision, Conceptualization. **Sam D. Clarke:** Writing – review & editing, Supervision, Conceptualization.

Declaration of competing interest

The authors declare that they have no known competing financial interests or personal relationships that could have appeared to influence the work reported in this paper.

Acknowledgements

Data availability

Data will be made available on request.

References

[1] Ross CA, Nash PT, Friesenhahn GJ. Pressure waves in soils using a split-Hopkinson pressure bar. Tech. rep., Southwest Research Institute San Antonio TX; 1986.

[2] Veyera GE. Uniaxial stress-strain behavior of unsaturated soils at high strain rates. Tech. rep., Wright Lab Tyndall Afb Fl; 1994.

[3] Gray III GT. Classic split Hopkinson pressure bar testing. ASM Handb 2000;8:462–76.

[4] Bragov A, Lomunov A, Sergeichev I, Tsembelis K, Proud W. Determination of physicomechanical properties of soft soils from medium to high strain rates. Int J Impact Eng 2008;35(9):967–76. http://dx.doi.org/10.1016/j.ijimpeng.2007.07.004.

[5] Luo H, Cooper WL, Lu H. Effects of particle size and moisture on the compressive behavior of dense Eglin sand under confinement at high strain rates. Int J Impact Eng 2014;65:40–55. http://dx.doi.org/10.1016/j.ijimpeng.2013.11.001.

[6] Barr AD. Strain-rate effects in quartz sand (Ph.D. thesis), University of Sheffield; 2016.

[7] Hopkinson B. X. A method of measuring the pressure produced in the detonation of high, explosives or by the impact of bullets. Philos Trans R Soc Lond Ser A Math Phys Eng Sci 1914;213(497–508):437–56. http://dx.doi.org/10.1098/rsta.1914.0010.

[8] Kolsky H. An investigation of the mechanical properties of materials at very high rates of loading. Proc Phys Soc Sect B 1949;62(11):676. http://dx.doi.org/10.1088/0370-1301/62/11/302.

[9] Kolsky H. Stress waves in solids. In: Dover books on physics. New York; 1963, http://dx.doi.org/10.1016/0022-460X(64)90008-2.

[10] Bragov A, Grushevsky G, Lomunov A. Use of the Kolsky method for confined tests of soft soils. Exp Mech 1996;36:237–42. http://dx.doi.org/10.1007/BF02318013.

[11] Ma Q-Y. Experimental analysis of dynamic mechanical properties for artificially frozen clay by the split Hopkinson pressure bar. J Appl Mech Tech Phys 2010;51(3):448–52. http://dx.doi.org/10.1007/s10808-010-0060-8.

[12] Yang R, Chen J, Yang L, Fang S, Liu J. An experimental study of high strain-rate properties of clay under high consolidation stress. Soil Dyn Earthq Eng 2017;92:46–51. http://dx.doi.org/10.1016/j.soildyn.2016.09.036.

[13] Konstantinov A, Bragov A, Igumnov L, Eremeyev V, Balandin VV, et al. Experimental study and identification of a dynamic deformation model of dry clay at strain rates up to 2500 s-1. J Appl Comput Mech 2022;8(3):981–95. http://dx.doi.org/10.22055/jacm.2022.39321.3387.

[14] Hallquist JO, et al. LS-DYNA keyword user's manual, vol. 970, Livermore Software Technology Corporation; 2007, p. 299–800.

[15] Church P, Cornish R, Cullis I, Gould P, Lewtas I. Using the split Hopkinson pressure bar to validate material models. Phil Trans R Soc A 2014;372(2023):20130294. http://dx.doi.org/10.1098/rsta.2013.0294.

[16] Cundall PA, Strack OD. A discrete numerical model for granular assemblies. Geotechnique 1979;29(1):47–65. http://dx.doi.org/10.1680/geot.1979.29.1.47.

[17] Busch CL, Tarefder RA. Evaluation of appropriate material models in LS-DYNA for MM-ALE finite element simulations of small-scale explosive airblast tests on clay soils. Indian Geotech J 2017;47(2):173–86. http://dx.doi.org/10.1007/s40098-016-0196-4.

[18] Eremeyev V, Balandin V, Bragov A, Konstantinov AY, Igumnov L, et al. Experimental study and numerical simulation of the dynamic penetration into dry clay. Contin Mech Thermodyn 2023;35(2):457–69. http://dx.doi.org/10.1007/s00161-023-01189-w.

[19] Lacome JL. Smooth particle hydrodynamics (SPH): a new feature in LS-DYNA. In: 6th international LS-DYNA users conference. 2000, p. 7–30.

[20] ISO. 14688-1: 2002: Geotechnical investigation and testing – Identification and classification of soil – Part 1: Identification and description. British Standards Institution; 2002.

[21] BSI. BS 1377-2: 1990: Methods of test for soils for civil engineering purposes – Part 2: Classification tests. 1990.

[22] Casagrande A. Classification and identification of soils. Trans Am Soc Civ Eng 1948;113(1):901–30. http://dx.doi.org/10.1061/TACEAT.0006109.

[23] Van Lerberghe A, Li KSO, Barr AD, Clarke SD. An open-source algorithm for correcting stress wave dispersion in split-Hopkinson pressure bar experiments - currently under review. Sensors 2024.

[24] Li KSO, Van Lerberghe A, Barr A. SHPB_Processing.py - An open-source Python algorithm for correcting stress wave dispersion in split-Hopkinson pressure bar experiments. 2024, http://dx.doi.org/10.15131/shef.data.24570565.v1.

[25] Tyas A, Pope DJ. Full correction of first-mode Pochammer–Chree dispersion effects in experimental pressure bar signals. Meas Sci Technol 2005;16(3):642. http://dx.doi.org/10.1088/0957-0233/16/3/004.

[26] Li KSO, Van Lerberghe A, Barr A, Clarke SD, Dennis AA. Split-Hopkinson pressure bar testing of water with partial lateral confinement - currently under review. Meas Sci Technol 2024.

[27] Mostafa KF, Liang RY. Numerical modeling of dynamic compaction in cohesive soils. 738–747. http://dx.doi.org/10.1061/41165(397)76.